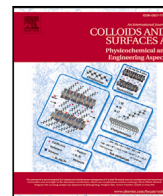Contents lists available at ScienceDirect

Colloids and Surfaces A: Physicochemical and Engineering Aspects

journal homepage: www.elsevier.com/locate/colsurfa

Modeling liquid–vapor phase change experiments: Cryogenic hydrogen and methane
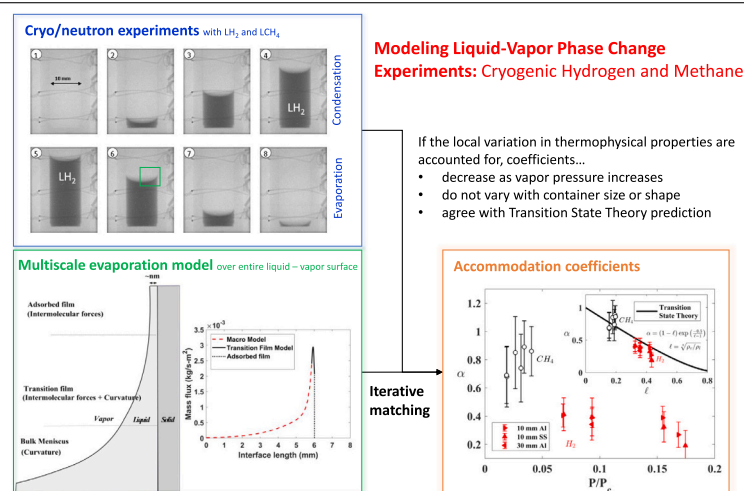
Kishan Bellur [a,b,*], Ezequiel F. Médici [b], James C. Hermanson [c], Chang Kyoung Choi [b], Jeffrey S. Allen [b]

[a] University of Cincinnati, Cincinnati, OH, USA
[b] Michigan Technological University, Houghton, MI, USA
[c] University of Washington, Seattle, WA, USA

GRAPHICAL ABSTRACT

ARTICLE INFO

ABSTRACT

Mass accommodation coefficients are essential inputs to kinetic models of liquid–vapor phase change, yet after nearly 100 years there remains significant discrepancy in reported values. These discrepancies have been attributed to a wall material or geometric dependency resulting in the need for an empirical correction factors. The lack of experimental results for cryogenic fluids poses a serious impediment to modeling/predicting propellant behavior for long term space missions. Using a combination of neutron imaging experiments and multi-scale modeling, mass accommodation coefficients for liquid hydrogen and methane are determined. When the local variation in thermophysical properties are accounted for, the experimentally derived accommodation coefficients for hydrogen are invariant to container size, material and evaporation rate. The discrepancy in prior measurements of the accommodation coefficient for other fluids can be alleviated by a multi-scale analysis that incorporates local variation in thermophysical properties. The values of accommodation coefficients for hydrogen and methane are consistent with generalized transition state theory. This suggests that a mass accommodation coefficient is a solely a function of the liquid–vapor density ratio, making it a fluid-independent property easily determined without the need for empirical correction factors as reported in previous investigations.

---

* Corresponding author at: University of Cincinnati, Cincinnati, OH, USA.
E-mail address: bellurkn@ucmail.uc.edu (K. Bellur).

1. Introduction

Kinetic theory has provided a basis for the understanding and modeling of liquid–vapor phase change for over a century. This is particularly important in cases where diffusive transport in the vapor is not the limiting factor. This includes pure, single component liquid–vapor phase-change and phase-change in the presence of significant contact line contributions [1,2]. Kinetic theory modeling of phase-change has also been shown to regularize the singularity at a moving contact line [3].

Kinetic models have been effective in capturing phase change, but the use of these models is still limited due to the fact that kinetic theory is based on equilibrium constructs. Despite the equilibrium basis, kinetic models over-predict evaporation and condensation [4,5]. The deviation from the theoretical rate of phase change is accounted for through the use of evaporation and condensation coefficients; also referred to as mass accommodation coefficients. Determining accurate values of evaporation/condensation coefficients has implications in many fields including space technology [1,6,7], atmospheric science and climate [8,9], aerosol transport [10,11] micro- and nano-scale thermal transport in MEMS applications [12–14].

Challenges with kinetic descriptions of phase-change include defining boundary conditions at the liquid–vapor interface and determining values of the accommodation coefficient. There is significant discrepancy in both the definition of accommodation coefficients and in the reported values [15–19]. A comprehensive model of liquid–vapor phase change requires implementation of a kinetic model with continuum descriptions of heat and mass transfer on the liquid side of the interface. A number of simplifying assumptions are included in many formulations, which makes quantitative validation of model predictions with experimental measurements difficult.

An opportunity to test the role of liquid surface modeling on derived values of accommodation coefficients arose out of a need by NASA. Accommodation coefficients are required to predict cryogenic propellant boil-off from orbital fuel depots for long-duration space missions. Of specific interest are liquid hydrogen and methane [6,20,21]. Neither the values of accommodation coefficients nor a technique to determine them existed. As a result, the coefficient was reduced to an arbitrary tuning parameter in CFD models. Values as low as 10^{-6} have been used to achieve numerical stability in these models [21–23]. Modeling phase change inside propellant tanks remains a challenge due to the uncertainty of accommodation coefficients and an inability to predict local interfacial thermodynamics [1,2,6,7,24]. A new technique for determining accommodation coefficients for hydrogen and methane was developed to directly address this need and is reported here.

The objectives of this study are three-fold. The first is to discuss the iterative methodology used to determine accommodation coefficients. The experiment and modeling details have been previously published [1,2,25–28]. This study is focused on how kinetic theory, continuum modeling, and experiment results were combined in order to extract accommodation coefficients. The second objective is an evaluation of how modeling choices affect the resulting value of accommodation coefficients. This discussion helps explain the significant discrepancy in reported values. Finally, the third objective is to report the values of the accommodation coefficient for evaporating hydrogen and methane. These values are independent of container size and geometry, but do depend on the thermodynamic state of the vapor. A comparison of the extracted accommodation coefficients to transition state theory is included. To the best of the authors' knowledge, these are the first published values of the accommodation coefficients for cryogenic propellants.

2. Modeling phase change using kinetic theory

Kinetic theory is a statistical description of the behavior of gases based on velocities of the constituent molecules. Under equilibrium conditions, the vapor can be modeled as an ideal gas that follows a Maxwell–Boltzmann distribution. This velocity distribution leads to an expression for flux of vapor molecules passing through a hypothetical plane [4].

$$j_v = \sqrt{\frac{m}{2\pi k_b}} \left(\frac{P_v^{\text{sat}}}{\sqrt{T_v}} \right) \tag{1}$$

P_v^{sat}, k_b, m, and T_v are saturation vapor pressure, Boltzmann constant, mass of a vapor molecule, and vapor temperature, respectively. Subscript v denotes the bulk vapor phase.

Applying kinetic theory to liquid–vapor phase change requires that an interface location be defined. The liquid–vapor interface is often treated as sharp with a density jump shown at location s_i in Fig. 1(a). A hypothetical plane to which kinetic theory is applied is located in the vapor at a distance Δs from the interface location [29]. The kinetic plane is denoted as s_{kp} in Fig. 1(a). Δs is arbitrary and is often assumed to be infinitesimal. A diffuse interface model, shown in Fig. 1(b), remedies the arbitrary location of s_{kp} since a value of Δs is determined from the density gradient easily estimated from molecular dynamics simulations [19]. The liquid–vapor surface thus becomes a region rather than a sharp interface. The intersection of the interfacial region and the bulk vapor is the location of the kinetic plane.

The net mass flux is the difference in evaporation, j_ℓ, and condensation flux, j_v, across the kinetic plane. At equilibrium these two fluxes are equal, $j_\ell = j_v$, and the bulk liquid temperature is equal to the bulk vapor temperature, $T_\ell = T_v$. During net phase change, $j_\ell \neq j_v$ and a temperature jump exists across the interfacial region [19]. A condensation flux, j_v, can be determined using Eq. (1) when P_v^{sat} is replaced by the bulk vapor pressure P_v. The evaporation flux is the molecular flux at the liquid–vapor interface at equilibrium using the liquid interfacial temperature, $T_{l,i}$. This flux is also described by Eq. (1) with $P_{v_{sat}}$ substituted with the $P_{v,l}$ and T_v substituted with $T_{l,i}$. The net mass flux is then

$$\dot{m}'' = j_\ell - j_v = \sqrt{\frac{m}{2\pi k_b}} \left(\frac{P_{v,l}}{\sqrt{T_{l,i}}} - \frac{P_v}{\sqrt{T_v}} \right) \tag{2}$$

where $T_{l,i}$ is the temperature of the interface on the liquid side, T_v is the temperature of the bulk vapor and $P_{v,l}$ is the equilibrium vapor pressure of the liquid at the interface at temperature $T_{l,i}$. This inherently non-equilibrium process of phase change is modeled using superposition of two seemingly unrelated fluxes: a non-equilibrium flux for condensation (j_v) and an equilibrium flux for evaporation (j_v). This is an inherent limitation in all kinetic theory models and is often overlooked.

Early experiments consistently measured phase change rates lower than those predicted by Eq. (2). This discrepancy is commonly attributed to reflection of vapor molecules at the interface [5,16,30]. Accommodation coefficients were introduced by Knudsen [31] to account for the difference between measured and theoretical flux.

$$\dot{m}'' = \sqrt{\frac{m}{2\pi k_b}} \left(\alpha_e \frac{P_{v,l}}{\sqrt{T_{l,i}}} - \alpha_c \frac{P_v}{\sqrt{T_v}} \right) \tag{3}$$

where α_e is the evaporation coefficient and α_c is the condensation coefficient. Eq. (3) is the known as the Hertz–Knudsen (HK) equation and it represents the difference in collisional frequency of vapor molecules on either side of the kinetic plane, though α_c and α_e apply to the interface region.

During steady evaporation or condensation, there is a net macroscopic drift of vapor molecules across the kinetic plane, either away from or towards the liquid–vapor interface, respectively. This alters the Maxwell–Boltzmann equilibrium velocity distribution in the vapor space at the kinetic plane location [5,32]. Schrage [5] developed a
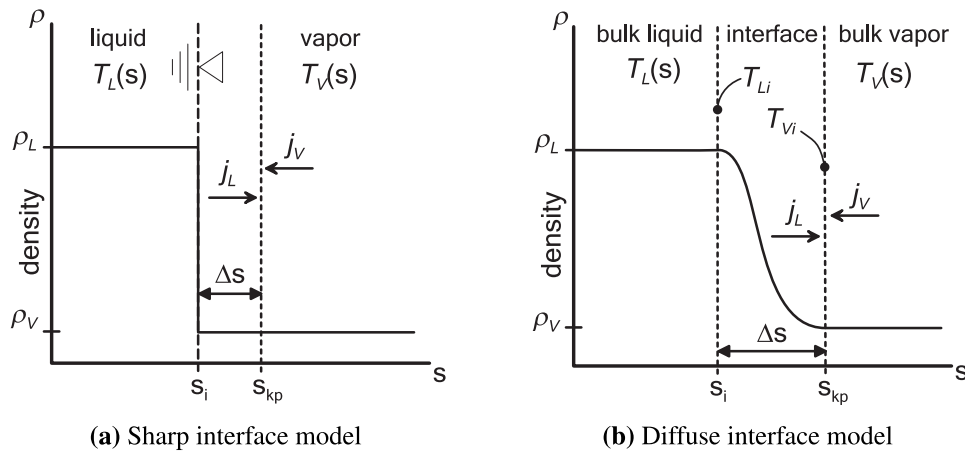
(a) Sharp interface model   **(b)** Diffuse interface model

Fig. 1. Two interface models for examining net mass flux to or from a liquid–vapor interface. The hypothetical kinetic plane is located in the vapor phase at s_{kp}. Net phase change is the difference in mass flux crossing the kinetic plane from liquid and vapor sides. Interfacial temperatures for the diffuse model are denoted with the subscript '*i*'.

correction factor, $D(\xi)$, to account for this drift velocity and applied it to the condensation flux term.

$$\dot{m}'' = \sqrt{\frac{m}{2\pi k_b}}\left(\alpha_e \frac{P_{v,l}}{\sqrt{T_{l,i}}} - D(\xi)\alpha_c \frac{P_v}{\sqrt{T_v}}\right) \qquad (4)$$

where

$$D(\xi) = e^{\xi^2} - \sqrt{\pi}\xi\left[1 + \mathrm{erf}(\xi)\right] \qquad (5)$$

ξ is the ratio of the drift velocity, w_0, to the most probable velocity of a vapor molecule in the bulk phase, c_R.

$$c_R = \sqrt{\frac{2k_b T_v}{m}} \qquad (6)$$

Here, m is the mass of a vapor molecule. For a gas or vapor in equilibrium at temperature T_v, the ideal gas model is equivalent to:

$$\frac{P_v^{\mathrm{sat}}}{\rho_v^{\mathrm{sat}}} = \frac{1}{2}c_R^2 \qquad (7)$$

The drift velocity, w_0, can be thought of as the net mass flux at the kinetic plane divided by the density of the vapor. Therefore, the drift velocity ratio, ξ, can be expressed as:

$$\xi = \frac{w_0}{c_R} = \frac{\dot{m}'' c_R}{2P_v^{\mathrm{sat}}} \qquad (8)$$

The mass flux dependency in Eq. (8) means that the solution of Eq. (4) is implicit when the drift flux correction is included. As noted by Carey [32], however, ξ is small for many evaporation and condensation processes. For $\xi \leq 10^{-3}$ the drift flux correction can be simplified to:

$$D(\xi) = 1 - \frac{\sqrt{\pi}}{2}\left(\frac{c_R}{P_v^{\mathrm{sat}}}\right)\dot{m}'' \qquad (9)$$

For the experiments reported herein, $\xi \approx 10^{-4}$ and the resulting net mass flux at the kinetic plane can be expressed as:

$$\dot{m}'' = \left(\frac{2\alpha_c}{2-\alpha_c}\right)\frac{P_v}{\sqrt{\pi}c_R}\left[\beta\frac{P_{v,l}}{P_v}\sqrt{\frac{T_v}{T_{l,i}}} - 1\right] \qquad (10)$$

where $\beta = \alpha_e/\alpha_c$. Eq. (10) is a normalized form of the Hertz–Knudsen–Schrage (HKS) equation. For simplicity and closure, it is common practice to assume that the condensation coefficient is equal to the evaporation coefficient ($\beta = 1$) [10,16,18,33–36]. The remaining coefficient, $\alpha_e = \alpha_c = \alpha$, is referred to as the *accommodation coefficient*.

If $\alpha_e = \alpha_c$ ($\beta = 1$), then the Hertz–Knudsen equation (3) and the Hertz–Knudsen–Schrage equations (10) are identical except for the kinetic prefactor. To alleviate confusion in the rest of this study, the coefficient computed without inclusion of drift velocity is denoted as $\underline{\alpha}$

and the drift velocity corrected value is denoted as $\hat{\alpha}$. The relationship between the kinetic prefactors is $\underline{\alpha} = 2\hat{\alpha}/(2 - \hat{\alpha})$ for $\xi < 10^{-2}$.

Variations of Eqs. (1)–(4) have been used to extract accommodation coefficients from carefully conducted experiments, but published values vary widely [10,15,16,18]. Marek and Straub [16] and Haynes et al. [15] report values for water that range three orders of magnitude with an upper limit of one. Persad and Ward [37] report values for water that exceed unity. Attempts to investigate and explain the discrepancy of these coefficients have not yielded a consensus. The variation in reported values has been attributed to many factors including difficulty in determining the interfacial temperature, container geometry, liquid impurities, dynamic surface tension, and renewing surfaces [16,17,38,39].

A significant observation in this regard was reported by Cammenga et al. [39] and reiterated by Marek and Straub [16]; which is values of the accommodation coefficients depend upon with the choice of material used for the liquid container. This suggested that wettability and interface curvature influenced experimentally determined evaporation rates and, subsequently, the values of derived accommodation coefficients. Others have observed variations in accommodation coefficients with the size of the liquid container or liquid drop [40–42]. Burrows [43] proposed a fit for the accommodation coefficient that was a function of the condensing surface area and an empirically determined shape factor [43–46]. Kapłon et al. [47] proposed an alternative correlation, as did Bryson et al. [48,49], but none of these correlations are universal with respect to surface area.

Extraction of accommodation coefficients from phase change experiments require interfacial temperature and pressure conditions to be known *a priori*. Direct interfacial measurements are difficult and attempts to place a sensor in the interface region invariably alter the local interface curvature and heat transfer characteristics [37]. A common assumption imposed for simplicity and closure is to set pressure ratio, $P_{v,l}/P_v$, in Eq. (10) equal to unity. This assumption may be appropriate for large liquid surfaces without significant curvature or contact line area relative to bulk surface area, but as noted by Hołyst et al. [50], evaporation is driven by small differences in pressure, which might explain the discrepancy in published values of evaporation coefficients.

Another nearly-universal simplification is to assume interfacial pressure and temperature are constant over the entire liquid surface with values corresponding to bulk liquid and vapor conditions [17,33,51–58]. This assumption quickly breaks down, however, if the liquid surface is a meniscus with thermal energy transferred through a container wall. The interface temperature cannot be maintained at a constant value due to the differences in heat conduction path length from the test cell wall to the liquid–vapor surface. The effects of curvature are addressed in the next section.
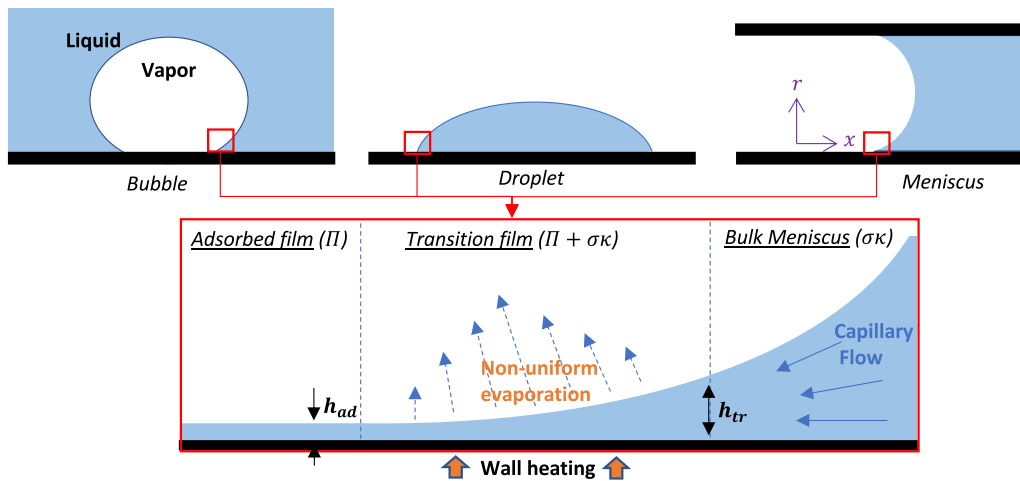
Fig. 2. Delineation by key contributions to pressure jump at the liquid–vapor surface. The adsorbed film region is strongly affected by disjoining pressure with characteristic film thickness $h_{ad} \sim$ nm. The transition film region is affected by disjoining pressure and capillarity.

2.1. Adaptation of the Kelvin equation

For a curved surfaces as shown in Fig. 2, the local thermophysics can vary along the liquid–vapor surface due to curvature and anisotropic stresses arising in thin liquid films. Fig. 2 delineates the different regions of a meniscus according to the dominant liquid pressure component. The interface shape of the bulk meniscus region is governed by capillary pressure. At sub-micron liquid thicknesses the disjoining pressure (net pressure reduction due to intermolecular forces) increases so that capillary and intermolecular forces become comparable. This mechanical effect reduces the local evaporation flux. In the nano-scale adsorbed film region, evaporation is further suppressed by disjoining pressure. In contrast, thermal resistance decreases with liquid thickness resulting in a higher heat flux from the wall through the liquid and a higher local evaporative flux in the transition film region. The interplay between thermal and mechanical effects generates a non-uniform evaporative flux with a peak occurring in the transition film region, an observation reported in numerous studies [35,59–62].

Wayner et al. [36] initiated the modern use of an adapted Kelvin equation to model the effect of curvature and disjoining pressure on phase change. Our starting point for this thermodynamic model is [34, 63,64]:

$$\ln\left(\frac{P_{v,l}}{P_{v,R}}\right) = \frac{\bar{M} h_{lv}}{\bar{R} T_v T_{l,i}}\left(T_{l,i} - T_v\right) + \frac{\bar{v}_l}{\bar{R} T_{l,i}}\left(\Pi + \sigma K + K \Delta\sigma_p\right) \quad (11)$$

where Π is disjoining pressure, σ is surface tension, K is interface curvature, $\bar{v}$ is molar volume, and h_{lv} is the latent heat of vaporization. This formulation is derived using the Gibbs–Duhem and Clapeyron equations and by integrating pressure from a reference state to the absorbed film region dominated by disjoining pressure. The reference state, denoted as $P_{v,R}$, is saturated vapor pressure over a bulk liquid layer where curvature and disjoining pressure are equal to zero. $P_{v,l}$ is the vapor pressure at the liquid interface temperature $T_{l,i}$. The change in surface tension due to pressure, $\Delta\sigma_p$, likewise is the difference between the planar, saturated state and the absorbed film. For this work it was assumed that $\Delta\sigma_p = 0$. Implicit in this derivation is the requirement that pressure and temperature jumps across the liquid–vapor surface are small and the molar density of the vapor is much smaller than the liquid.

The coefficients on the temperature and pressure potentials in Eq. (11) can be related to the most probable velocity of a vapor molecule, c_R.

$$\frac{\bar{v}_l}{\bar{R} T_v} = \frac{\bar{M}}{\rho_l \bar{R} T_v} = \frac{2}{\rho_l c_R^2} \quad (12)$$

The Kelvin equation can then be written as:

$$\ln\left(\frac{P_{v,l}}{P_{v,R}}\right) = \left(1 - \frac{T_v}{T_{l,i}}\right)\left(\frac{h_{lv}}{c_R^2/2}\right) + \left(\frac{T_v}{T_{l,i}}\right)\left(\frac{\Pi + \sigma K}{\rho_l c_R^2/2}\right) \quad (13)$$

The log of the pressure ratio can be expanded in a Taylor series centered at unity, which can be truncated after the first term if $0.975 < P_{v,l}/P_{v,R} < 1.025$. Using this approximation along with Eq. (7), the Kelvin equation reduces to:

$$\frac{P_{v,l}}{P_{v,R}} = 1 + \left(1 - \frac{T_v}{T_{l,i}}\right)\left(\frac{\rho_v^{sat} h_{lv}}{P_{v,R}}\right) + \left(\frac{T_v}{T_{l,i}}\right)\left(\frac{\rho_v^{sat}}{\rho_l}\right)\left(\frac{\Pi + \sigma K}{P_{v,R}}\right) \quad (14)$$

A common practice is to directly substitute equation (14) for the pressure ratio $P_{v,l}/P_v$ in the kinetic model of phase change. But this forces $P_v = P_{v,R}$ and implies thermal equilibrium and $\Pi = K = 0$ due to the choice of integrands used to derive equation (11). The reference state selected was saturation over a planar, bulk liquid layer, that may not exist relative to the actual liquid surface being studied; for example a highly curved meniscus or drop. A more appropriate reference state might be the equilibrium state (thermal and mechanical) in which interfacial effects on the normal stress condition are considered *a priori*, but the derivation is beyond the scope of this paper.

A reasonable alternative to arbitrarily setting $P_v = P_{v,R}$ is to assume, for a relatively large liquid surface, that the reference state is equivalent to the saturation state of the vapor, $P_{v,R} = P_v^{sat}(T_v)$. With this assumption the pressure ratio in Eq. (10) becomes:

$$\frac{P_{v,l}}{P_v} \approx \frac{P_v^{sat}}{P_v} + \left(1 - \frac{T_v}{T_{l,i}}\right)\left(\frac{\rho_v^{sat} h_{lv}}{P_v}\right) + \left(\frac{T_v}{T_{l,i}}\right)\left(\frac{\rho_v^{sat}}{\rho_l}\right)\left(\frac{\Pi + \sigma K}{P_v}\right) \quad (15)$$

subject to the following conditions:

1. $P_{v,R} = P_v^{sat}(T_v)$,
2. ρ_v^{sat}, h_{lv} are determined at T_v.
3. $0.975 < P_{v,l}/P_v^{sat} < 1.025$.

Eqs. (10) and (15) are sufficient to determine the accommodation coefficient, α, from the cryogenic experiments if T_v, $T_{l,i}$, P_v, and $P_{v,l}$ are known. The bulk vapor properties, T_v and P_v, are relatively easy to measure, but the interface properties, $T_{l,i}$ and $P_{v,l}$, must be inferred from thermal-fluid modeling of the phase-change experiments.

3. Cryogenic phase-change experiments

Cryogenic hydrogen and methane phase-change experiments were specifically designed to test the dependence or independence of derived
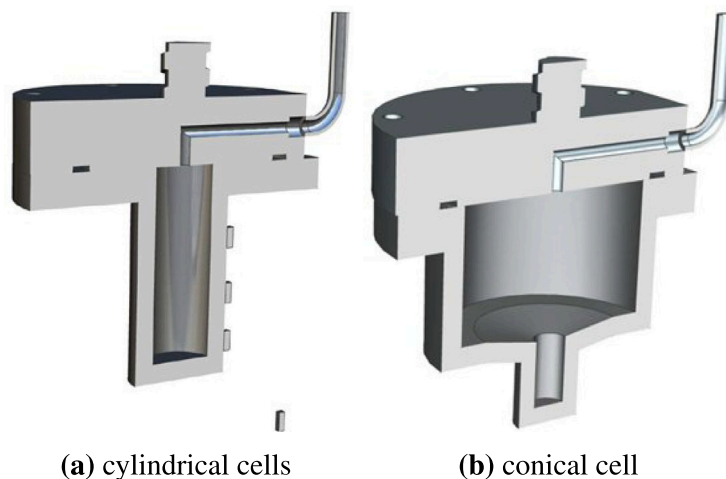
(a) cylindrical cells **(b)** conical cell

Fig. 3. Two types of test cell geometries were used (a) cylindrical and (b) conical. The cylindrical cells of various materials (Al 6061 and SS 316) and sizes (10 mm and 30 mm) were tested.

accommodation coefficients on surface area, contact line area, wettability, and curvature. Evaporation and condensation rates were measured using neutron imaging at the NIST Center for Neutron Research (NCNR) in Gaithersburg, MD. Neutron scattering cross-sections are large for hydrogen and methane but small for aluminum and stainless steel. This allowed for imaging liquid hydrogen and methane through both the cryostat and test cell. Two different test cell configurations, shown in Fig. 3, and two materials (Al 6061 and 316L SS) were used to investigate the role of liquid surface area, surface curvature, and apparent contact line length on the derived value of accommodation coefficients. Cylindrical test cells with an inner diameter of 10 mm and 30 mm were fabricated from 6061 Al along with a 10 mm 316L SS. The conical test cell was fabricated from 6061 Al with 5 mm and 30 mm diameters and a 10 degree conical transition.

Cryogenic hydrogen or methane vapor was introduced into an evacuated container. Vapor temperature or pressure were then varied to initiate condensation and evaporation. Neutron imaging was used to measure the change in liquid volume. This is an attenuation-based measurement and pixel intensity is related to the thickness of liquid the neutrons traverse. Fig. 4(a) is a sequence of images showing steady condensation and then evaporation of liquid hydrogen in a 10 mm Al 6061 cylinder. The liquid surface curvature in the 10 mm diameter was large $K_{10\,mm} \approx 400\,m^{-1}$ for a perfectly wetting liquid. The curvature in the 30 mm diameter test cell is $K_{30\,mm} \approx 67\,m^{-1}$ while the curvature in the 5 mm diameter section of the conical cell is $K_{5\,mm} \approx 1250\,m^{-1}$. The curvature in the 10 degree transition portion of the conical cell is negligible. Ideally, and if the models are correctly formulated, the values of accommodation coefficients derived from experiments are independent of the choice of test cell used for experiments.

Experiments were conducted over a range of saturation pressures from 80 to 220 kPa. A typical condensation–evaporation test is shown in Fig. 4(b). The measured experimental data consists of neutron images, wall temperatures and vapor pressures [27]. Evaporation/ condensation rates were obtained by image processing. Measured rates of phase change vary between test cells even at the same vapor pressure because of changes in heat transfer to/from the cryostat. Details on the neutron imaging experiments, image processing, and data analyses are available in Bellur et al. [1,24,27,65]. In addition, the entire dataset is publicly available [28].

4. Modeling the cryogenic experiments

A comprehensive, multi-scale heat transfer model has been developed to determine local thermophysical quantities, $T_{l,i}$ and $P_{v,l}$, along

the evaporating liquid hydrogen and liquid methane surfaces. Phase change was modeled using a multi-scale approach comprised of two submodels, one for the macro-scale meniscus region and the other for the micro-scale transition film region as delineated in Fig. 1. In addition, a thermal transport model is used to determine the wall temperature boundary conditions. A full description of the submodels are available in previously published work [2,26,66] and a brief overview is provided below.

### 4.1. Inner wall temperature boundary conditions

The inner wall temperatures are required boundary conditions, but could not be directly measured. Hence, a thermal transport model was built in ANSYS/Fluent model to translate the experimentally measured discrete outer wall temperature measurements into an inner wall temperature distribution. This model accounted for heat conducted along the test cell holder and through the helium in the cryostat well. The heat transfer along the test cell holder included five contact resistances that changed with each test configuration. Configuration-specific contact resistances were determined by applying the ANSYS/Fluent thermal transport model to an evacuated test cell subjected to thermal cycling. The thermal transport model was coupled with the multiscale phase change model to determine the inner wall temperature distribution as shown in Fig. 4(c). The inner wall temperature minima is observed in the contact line region.

4.2. Macro-scale meniscus region

The local interface temperature, $T_{l,i}$, and pressure, $P_{v,l}$, along the liquid–vapor interface were determined by modeling heat transfer through the liquid domain. The shape of the liquid–vapor interface was determined using a Young–Laplace fit to the neutron images [65]. For all tests conducted, the Rayleigh number was well below the critical value for natural convection and the Peclet number was less than 1. Hence, heat transport to the liquid–vapor interface was by conduction through the liquid. A 2D axisymmetric, steady state heat conduction model was developed in MATLAB and evaluated using the built-in finite element solver. A uniform mesh with 5 µm triangular elements was used as a compromise between speed and accuracy. The solution of the macro-scale meniscus submodel yields the local mass flux $\dot{m}''$ and local interfacial temperature $T_{l,i}$ across the bulk meniscus [2,66].
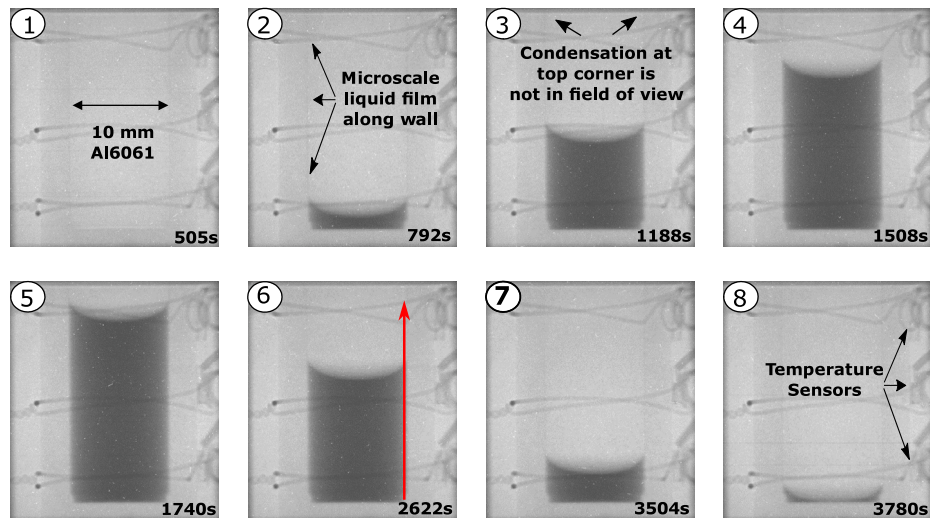
(a) Condensation/evaporation images
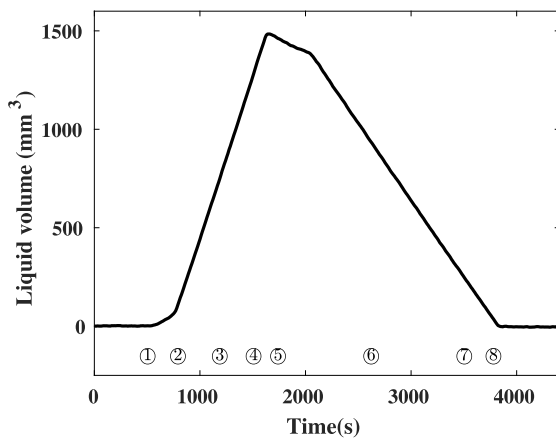
(b) Rate of condensation and evaporation
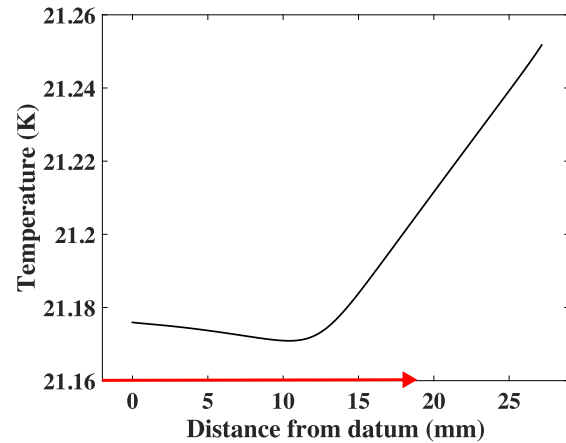
(c) Inner Wall Temperature Distribution

Fig. 4. (a) Condensation and evaporation of liquid hydrogen at $P_v^{\text{sat}} = 120$ kPa in a 10 mm diameter Al 6061 container. The cryostat temperature is used to control phase change while the vapor pressure is held constant. (b) Total liquid volume determined through image processing. The slope of the linear sections represent condensation/evaporation rates. (c) Inner wall temperatures determined from the thermal transport model. The red arrow in the x-axis corresponds to the red arrow in image 6 of 4(a). The datum is the bottom of the test cell and the contact line region is located at 10 mm. For this test, $T_v = 20.98$ K.

4.3. Micro-scale transition film region

An axisymmetric thin-film evolution equation was derived in cylindrical coordinates. The evolution equation includes disjoining pressure, local curvature, and thermocapillary stresses [2,66]:

$$h_{xxx} - \frac{3h_{xx}^2 h_x}{1 + h_x^2} - \frac{h_{xx}h_x}{(R-h)} + \frac{h_x\left(1 + h_x^2\right)}{(R-h)^2} + \frac{\gamma}{\sigma}\left(\frac{1 + h_x^2}{R-h} + h_{xx}\right)\frac{dT_i}{dx}$$
$$+ \frac{1}{\sigma}\left(1 + h_x^2\right)^{\frac{1}{2}}\left(\frac{dP_l}{dx} + \frac{d\Pi}{dx}\right) = 0 \tag{16}$$

Here, h is liquid film thickness normal to the container wall, R is the radius of the container, $\gamma = d\sigma/dT$. The disjoining pressure, Π, is modeled using the polynomial expression A/h^3 where A is the Hamakar constant. Similar to the macro-scale submodel, P_l and $T_{l,i}$ are determined through mass and heat balances. Derivation of Eq. (16) and solution methodology are described in Bellur et al. [2].

The transition film region is treated as a discretized set of control volumes in order to determine local values of the pressure gradient dP_l/dx. Liquid flow in the transition film is modeled using the lubrication approximation:

$$\frac{1}{r}\frac{\partial}{\partial r}\left(r\frac{\partial u}{\partial r}\right) = \frac{1}{\mu_l}\frac{dP_l}{dx} \tag{17}$$

A no-slip condition is applied at the wall ($r = R$) and a tangential stress balance equal to $d\sigma/dx$ is applied at the liquid–vapor interface ($r = R - h$). The solution for the velocity, $u(r)$, from Eq. (17) is used to determine a mass flow rate through discrete control volumes in the transition film region.

$$\dot{m}_{cv} = 2\pi \int_{R-h}^{R} \rho_l u(r)r\,dr \tag{18}$$

The mass flow rates entering and exiting the control volumes are balanced by the evaporative flux evaluated using the kinetic model (Eqs. (10) and (15)).

An energy balance applied to the same set of discretized control volumes is used to determine $T_{l,i}$. The temperature boundary condition at the inner wall, T_w is determined in the same manner as for the macro-scale submodel. Steady heat conduction through the liquid film is:

$$k_l\frac{\partial}{\partial r}\left(r\frac{\partial T}{\partial r}\right) = 0 \tag{19}$$
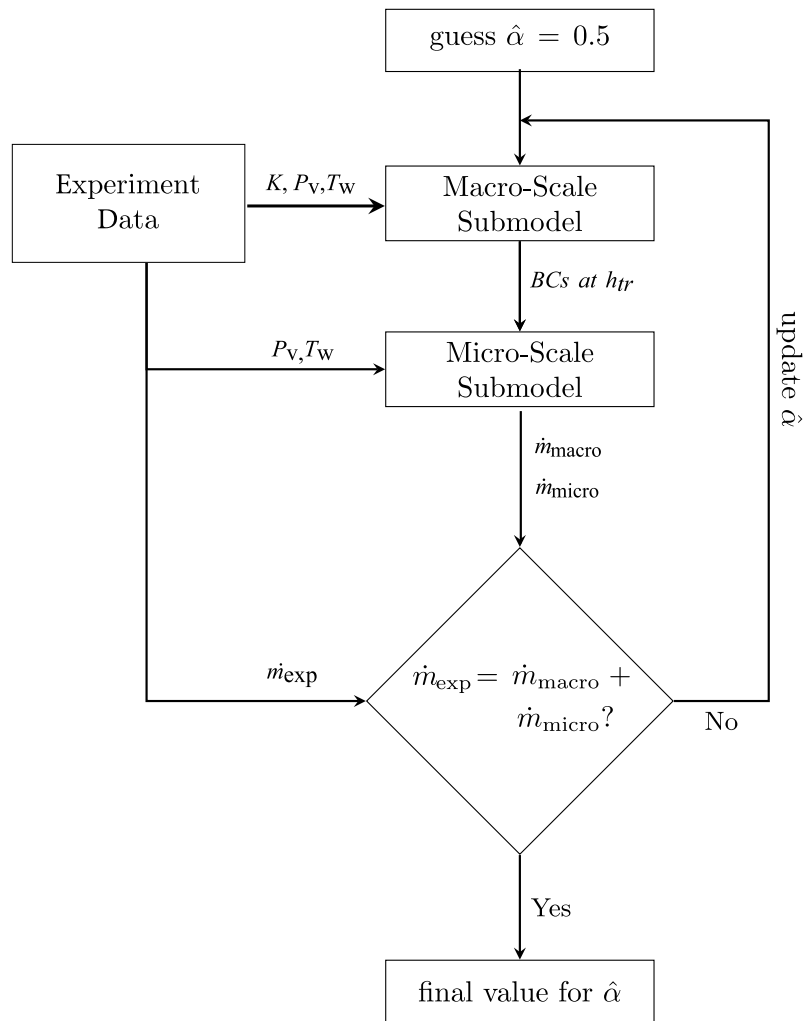
Fig. 5. Algorithm used to solve for $\hat{\alpha}$ begins with a guess of 0.5. Using experimental data (interface shape, wall temperature and vapor pressure) as inputs, the macroscale submodel is solved first and is truncated at h_{tr}. The end point conditions from macroscale submodel is used as a starting point for the microscale model ensuring continuity of mass flux and temperature profiles. The microscale submodel is solved in a direction of reducing thickness till an adsorbed film (h_{ad}) is reached. At the end of each submodel, the local mass flux is integrated over the interface to obtain $\dot{m}_{macro}$ and $\dot{m}_{micro}$. $\hat{\alpha}$ is determined iteratively such that $\dot{m}_{exp} = \dot{m}_{macro} + \dot{m}_{micro}$.

At the wall ($r = R$), the temperature is that determined using the exterior temperature measurements and the ANSYS/Fluent model of the cryostat. The heat conduction to the liquid–vapor interface is balanced by the rate of phase change.

$$k_l \frac{dT}{dr}\bigg|_{r=R-h} = \dot{m}'' h_{fg} \qquad (20)$$

The interfacial temperature distribution in the transition film region is obtained by integrating Eq. (19).

$$T_{l,i}(x) = -\frac{h_{fg}}{k_l}\left(R - h\right)\ln\left(\frac{R}{R-h}\right)\dot{m}'' + T_w(x) \qquad (21)$$

where $T_w(x)$ is the inner wall temperature distribution.

The evolution equation (16) is integrated from h_{tr}, where the disjoining pressure effects are negligible, to the adsorbed film where $h_x = 0$ and disjoining pressure effects are dominant. This integration path is opposite to most previous solutions which integrate from the absorbed film towards the bulk meniscus. The traditional approach exhibits an extreme sensitivity to the choice of a boundary condition for h_{xx} in the absorbed film region. The approach used here allows for closure without forcing the rate of phase change to be zero in the absorbed film region [2].

4.4. Solution scheme

The solution of the multi-scale modeling approach is outlined in Fig. 5. It begins with evaluation of the macro-scale submodel. Local temperature and mass flux profiles are solved from the center of the meniscus to a predetermined "cut off" point defined to be the entrance of the transition region where the film thickness is h_{tr} (see Fig. 1). The micro-scale submodel is then evaluated from h_{tr} to the point where the liquid–vapor interface slope reaches zero. The liquid film is considered to be an adsorbed film when $h_x = 0$.

The "cut-off" value of $h_{tr} = 10\,\mu m$ was selected for two reasons. First, at this liquid film thickness disjoining pressure is < 0.01% of the capillary pressure for all test configurations. Second, 10 μm is the optical limit of the imaging system with which local liquid–vapor interface curvature is measured. Continuity of film thickness, film slope, and temperature is maintained at h_{tr}.

5. Interfacial temperature and mass flux profiles

A typical profile of the calculated interfacial temperature jump along an evaporating hydrogen surface is shown in Fig. 6(a). The temperature jump and the mass flux evidently reach a peak in the
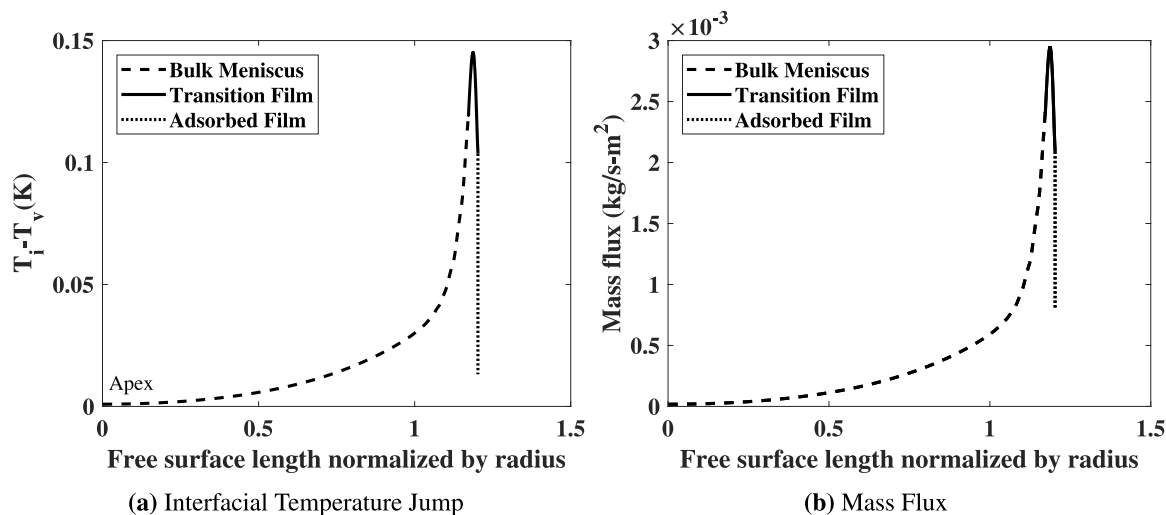
Fig. 6. Predicted liquid–vapor interface temperature jump and mass flux profiles for an evaporating hydrogen meniscus in a 10-mm diameter aluminum container at $P_v = 121.3$ kPa.

transition film region. The existence of a non-uniform temperature jump results in thermocapillary effects which are accounted for using a free surface boundary condition in the mass balance of micro-scale sub-model. For purposes of the current discussion, the multi-scale approach can be thought of as a tool to obtain the local interfacial temperature (Fig. 6(a)) and mass flux (Fig. 6(b)) along the liquid–vapor interface. The local mass flux is integrated over the interfacial area to obtain the net evaporation rate. The drift-velocity corrected accommodation coefficient $\hat{\alpha}$ is determined by iteratively matching the evaporation rates between the multi-scale model and experiments.

Fig. 6(a) presents a challenge to the long-established thought that a pure liquid–vapor interface cannot exhibit a temperature variation along the surface due, in part, to kinetic theory. Any temperature perturbation is thought to be saturated by localized evaporation and condensation. This may well be the case for large, flat liquid surfaces with little to no heat transfer and a 90° contact angle; in other words, the liquid–vapor surface is in thermal equilibrium. The cryogenic hydrogen and methane evaporation experiments stand in contrast to this equilibrium-based premise because of heat transfer from the container wall through the liquid. The heat conduction path through the liquid varies with a long conduction path to the meniscus centerline and a very short conduction path through the transition film region. This sustained heat transfer results in a liquid–vapor interface that is not in thermal equilibrium.

6. Accommodation coefficients for hydrogen and methane

The primary complication in evaluating all kinetic theory expressions is that the interfacial liquid temperature, $T_{l,i}$, and coefficients α_c and α_e are unknown in Eqs. (10) and (15). Even if $T_{l,i}$ is measured or approximated, there remain two unknowns, α_c and α_e. This necessitates the assumption that $\beta = 1$ in Eq. (10). This assumption is also necessary since the cryogenic phase-change experiments were conducted in an open configuration and there are insufficient constraints to determine both coefficients.

Values of $\hat{\alpha}$ derived for a range of evaporation test conditions and test cell configurations are shown in Table 1, and plotted against reduced vapor pressure in Fig. 7. Uncertainties in $\hat{\alpha}$ are due to uncertainties arising from temperature, pressure and neutron imaging measurements [66]. The dominant factor in the uncertainty is the outer wall temperature measurements. For hydrogen tests at 20 K this was ±0.25 K. For methane tests at 100 K this was ±1 K. There is also ambiguity in estimates of disjoining pressure. Sensitivity studies to variations in disjoining pressure were examined by varying the Hamaker constant

Table 1

Values of $\hat{\alpha}$ for a range of test conditions. $\dot{m}_{exp}$ is the experimentally determined evaporation rate. Test Cell designations are 1 : 10 mm Al, 2 : 10 mm SS, 3 : 30 mm Al.

	P_v, kPa	Test cell	$\dot{m}_{exp}$, µg/s	$\hat{\alpha}$
	88.90	1	55.20	0.41 ± 0.08
	88.32	2	17.27	0.41 ± 0.11
	121.30	1	55.50	0.39 ± 0.07
	120.90	2	16.43	0.40 ± 0.13
H_2	121.94	3	102.70	0.34 ± 0.11
	201.05	1	93.12	0.39 ± 0.08
	201.96	2	21.39	0.32 ± 0.11
	218.92	1	77.31	0.27 ± 0.09
	226.84	2	76.31	0.19 ± 0.11
	87.16	1	28.35	0.69 ± 0.20
	88.01	1	27.10	0.68 ± 0.21
CH_4	121.88	1	11.31	0.85 ± 0.25
	144.58	1	72.92	0.74 ± 0.24
	157.57	1	164.03	0.89 ± 0.19
	186.62	1	50.20	0.86 ± 0.18

by an order of magnitude. This variation changed the thickness of the absorbed film by 40%, but the resulting changes in $\hat{\alpha}$ were less than 0.1%.

The accommodation coefficients determined for methane are greater than those for hydrogen, which is consistent with prior molecular dynamics simulations that indicate $\hat{\alpha}$ increases with increasing molecular weight [67]. $\hat{\alpha}$ for hydrogen decreases with increasing vapor pressure. This decrease is consistent with both molecular dynamics studies [68,69] and experiments [16]. At low P_v, the mean free path is high. Hence, a molecule that leaves the liquid and enters the vapor phase has a very low probability of interacting with another vapor molecule before striking the container wall. In other words, the molecule has a lower probability of reflection resulting in a higher $\hat{\alpha}$. As P_v increases, the mean free path decreases and molecules that leave the liquid have a very high probability of reflection resulting in a lower value of $\hat{\alpha}$. This can be easily verified by looking at the limit of $P_v \to P_c$ where $\Delta\rho \to 0$. At the critical point, there is no potential for phase change and $\hat{\alpha}$ must theoretically reduce to zero.

The key observation from Table 1 and Fig. 7 is that $\hat{\alpha}_{H2}$ appears to be invariant to container size and material when curvature, disjoining pressure and drift velocity are considered in the underlying multi-scale model, at least to within the experimental uncertainty. Values of $\hat{\alpha}_{H2}$ are 0.4 at $P_v = 121$ kPa even though evaporation rates vary by an
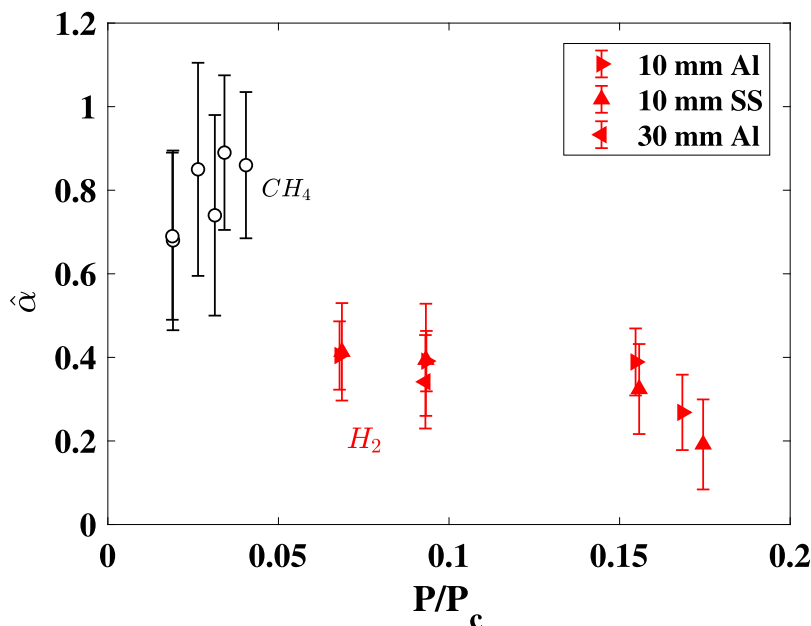
Fig. 7. The hollow circles denote methane evaporation tests and filled triangles are for hydrogen. Orientation of the triangle corresponds to different test containers. Only one container (10 mm Al) was used in the methane tests.
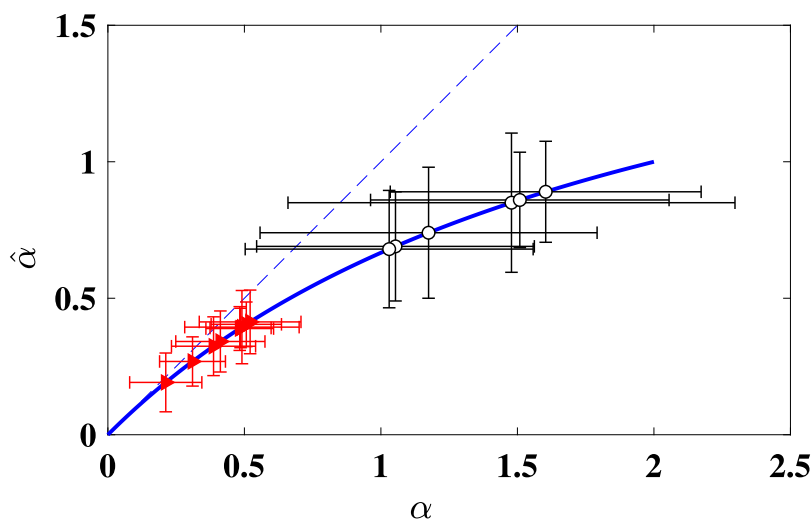

Fig. 8. Comparison of the accommodation coefficient computed with ($\hat{\alpha}$) and without ($\underline{\alpha}$) the drift velocity correction. Methane values are shown by hollow circles while the hydrogen values are shown by filled triangles.

order of magnitude across the three test cells. Methane evaporation data is only available for the 10 mm aluminum test cell, but the authors anticipate a similar response.

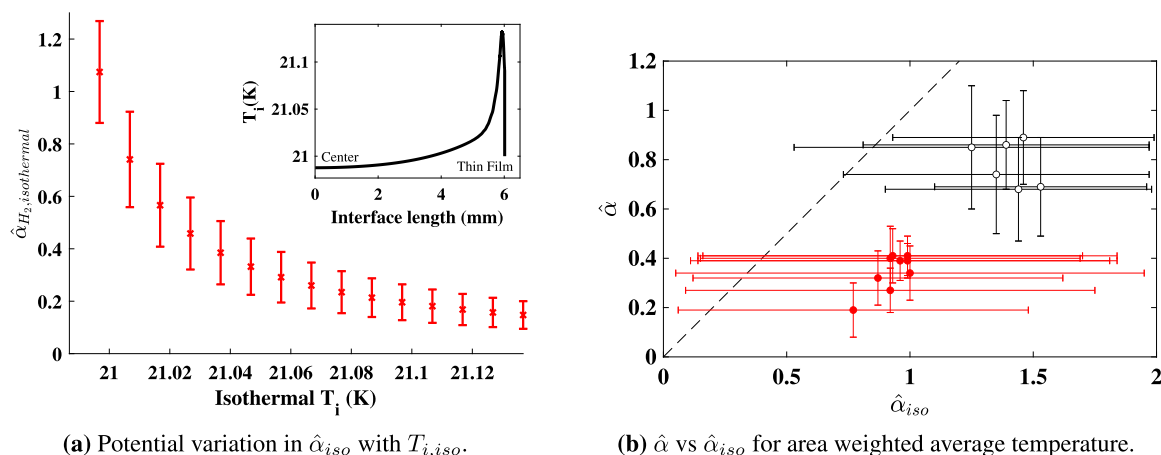*6.1. Influence of drift velocity correction*

A comparison between $\underline{\alpha}$ and $\hat{\alpha}$ for both hydrogen and methane is shown in Fig. 8. The methane values are indicated by hollow circles and hydrogen by filled triangles. The agreement between $\hat{\alpha}$ and $\underline{\alpha}$ is within experimental uncertainty for accommodation coefficients below 0.4. This suggests that the drift velocity correction might be negligible for the hydrogen experiments. However, there is significant deviation between $\underline{\alpha}$ and $\hat{\alpha}$ for the methane experiments. The uncertainty in $\underline{\alpha}$ is generally greater than the corresponding value of $\hat{\alpha}$. This is simply due to the scaling $\underline{\alpha} = 2\hat{\alpha}/(2 - \hat{\alpha})$. The maximum and minimum values of $\hat{\alpha}$ were found by iterative matching with experimental uncertainty.

Studies that do not incorporate a drift velocity correction have reported values of accommodation coefficients greater than unity [37]

even though these values ostensibly violate mass conservation. This is also apparent in Fig. 8 where $\underline{\alpha}$ is greater than 1 when $\hat{\alpha}$ is greater than 0.5. The possibility of violating mass conservation combined with the fact that an equilibrium distribution is used to model an inherently non-equilibrium process has raised concerns over the validity of the Hertz–Knudsen expression to model liquid–vapor phase change. Schrage's approach to drift velocity correction, on the other hand, has been validated with molecular dynamic simulations [68].

6.2. Effect of the isothermal interface assumption

Most prior studies of continuum-based modeling of liquid–vapor phase change have assumed a constant temperature over the entire liquid surface, often setting it equal to saturation and/or bulk vapor conditions [17,33,51–58]. This reduces the liquid–vapor interface to an isothermal boundary condition for the kinetic model, which for a flat interface implies a uniform phase change flux. There are a number

(a) Potential variation in $\hat{\alpha}_{iso}$ with $T_{i,iso}$.

(b) $\hat{\alpha}$ vs $\hat{\alpha}_{iso}$ for area weighted average temperature.

Fig. 9. (a) Using a typical range of T_i as seen from the 121 kPa hydrogen evaporation test in 10 mm Al cell. The uncertainty is experimental. (b) Comparison of the accommodation coefficient computed with ($\hat{\alpha}_{iso}$) and without ($\hat{\alpha}$) the isothermal temperature assumption for an area weighted average temperature. $\hat{\alpha}_{iso}$ is larger than the corresponding $\hat{\alpha}$ using an area weighted average for $T_{i,iso}$. The uncertainty in $\hat{\alpha}_{iso}$ is larger due to added contribution from the estimation of a single-point, isothermal temperature. Upper and lower bounds correspond to minimum and maximum isothermal temperature choices, respectively.

of reasons for using this assumption including simplicity in thermal modeling and the commonly held presumption that a pure liquid–vapor system cannot sustain a temperature gradient along an evaporating or condensing interface. If $T_{l,i}$ = constant (henceforth called $T_{i,iso}$), then the accommodation coefficient (denoted as $\hat{\alpha}_{iso}$) can be determined using Eq. (10) without the need for a continuum model of heat transfer through the liquid.

For the test conditions shown in Fig. 6(a) and the inset of Fig. 9(a), the computed interfacial temperature jump, $T_{l,i} - T_v$, varies between 10^{-5} K and 0.15 K. A representative isothermal interface temperature jump, $T_{i,iso} - T_v$, could be selected based on two bounding values: a minimum value at the axisymmetric center of the interface or a maximum value at the container wall in the thin film region. For hydrogen at 121.3 kPa in the 10 mm Al test cell, the minimum $T_{i,iso}$ is 21.0 K while the maximum value is 21.13 K. Accommodation coefficients determined through this forced isothermal approach are referred to as $\hat{\alpha}_{iso}$. Fig. 9(a) shows that $\hat{\alpha}_{iso}$ can vary by an order of magnitude based solely on the choice of $T_{i,iso}$. The area weighted average value of the interfacial temperature jump $T_{i,iso} - T_v$ is generally low (around 0.01 K) due to the large area contribution from the bulk meniscus as opposed to the small transition region area. Values of $\hat{\alpha}_{iso}$ computed for three different choices of $T_{i,iso} - T_v$ with data from the three different test cells are shown in Table 2. For $T_{i,iso} - T_v$ = 0.01, K the values of $\hat{\alpha}_{iso}$ decrease by approximately 13% when the test cell diameter is increased from 10 to 30 mm keeping the material constant. When the material is changed from aluminum to stainless keeping the size constant, $\hat{\alpha}_{iso}$ decreases by approximately 50%. The isothermal interface assumption therefore inherently introduces material and size dependence on the accommodation coefficient.

Therefore, it is not surprising that prior studies that used an isothermal approach perhaps resorted to empirical correction factors [43–49] or geometric scaling [42]. These findings provide possible explanations for the three orders of magnitude variation reported in literature [16]. The concept of an isothermal meniscus, used by many and generally obtained from equilibrium constructs, can lead to erroneous results even when the temperature variations are small (< 0.2 K).

6.3. Comparison to a fluid-independent framework

Nagayama and Tsuruta [70] developed a generalized equation for the mass accommodation coefficient using transition state theory and molecular dynamics.

$$\alpha = (1 - \ell)\, e^{-\ell/2(1-\ell)} \tag{22}$$

Table 2
Variation in $\hat{\alpha}_{iso}$ with both interfacial temperature jump ($T_{l,i} - T_v$) and choice of test cell at approximately the same vapor pressure.

Test cell	P_v (kPa)	$T_{l,i} - T_v$		
		0.01	0.1	0.2
10 mm Al	121.3	1.02	0.19	0.10
30 mm Al	121.9	0.87	0.14	0.07
10 mm SS	120.9	0.47	0.06	0.03

where ℓ is the cube root of the density ratio.

$$\ell = \left(\frac{\rho_v}{\rho_l}\right)^{1/3} \tag{23}$$

where ρ_v and ρ_l are the bulk vapor and liquid densities, respectively. Fig. 10 compares the values of $\hat{\alpha}$ from the cryogenic experiments against Eq. (22). Values of $\hat{\alpha}$ for methane are in excellent agreement with the theory of Nagayama and Tsuruta [70]. The agreement with hydrogen data is also good with measured values slightly below those predicted by Eq. (22). A select set of accommodation coefficients from other sources indicate a trend with ℓ that is consistent with Eq. (22). Experiments with water have yielded values close to unity [37,58], but these tests were conducted at approximately 1 kPa vapor pressure at which $\ell \approx 0$. Additional studies shown in Fig. 10 are based on molecular dynamics [19,42,71] and ℓ is estimated from number densities.

There are three potential reasons for the slight deviations in the case of hydrogen. First, the ideal gas simplifications may not strictly hold for hydrogen where the ratio of liquid-to-vapor mass density is relatively small and the vapor is close to saturation conditions. The compressibility factor for hydrogen at 20 K is estimated to be $Z = 0.91$ [72]. Second, hydrogen was assumed to be in the para state and transition to ortho was not considered in the energy balance. This assumption is based on an equilibrium para concentration that is > 99% at the normal boiling point with the time-scale for self-conversion on the order of weeks [73,74]. Finally, $\hat{\alpha}$ is assumed uniform over the interface even though the mass flux and interfacial temperature are not. This effectively makes the value of $\hat{\alpha}$ a meniscus-area averaged value. The density of the liquid in the transition and adsorbed film regions could vary from the bulk meniscus region, which based on Eq. (22) ought to result in a non-uniform value of the accommodation coefficient over the liquid–vapor interface. Future investigations into all three effects are recommended.
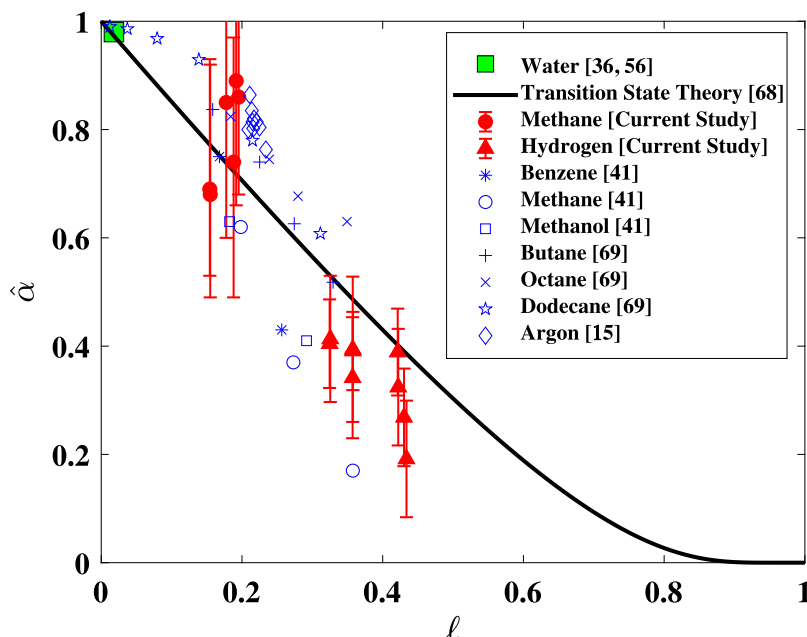
Fig. 10. The values of $\hat{\alpha}$ for methane and hydrogen are represented by red circles and triangles respectively. Prior reported data for other fluids are also shown. The data shows good agreement with the generalized fluid independent transition state theory prediction (Eq. (22)) represented by the solid line.

7. Summary and conclusion

Mass accommodation coefficients have generated considerable debate due to the wide range of reported value for seemingly similar experiments. Explanations for this discrepancy vary. Some investigators claim contamination or improper experiments while others argue a need for geometric shape factors. Based on a combination of neutron imaging experiments of hydrogen and methane evaporation with complementary multi-scale modeling, some portion of this discrepancy is found attributable to long-held convictions arising from equilibrium arguments. That is, a pure liquid–vapor interface has a uniform temperature during phase change. This is convenient when examining kinetic theory, but it reduces the liquid phase to a passive continuum boundary and neglects the role of heat transfer. When local liquid temperature and pressure variations are taken into account, experimentally derived accommodation coefficients for hydrogen exhibit an invariance to container size, material, and evaporation rate. Neglecting heat transfer, local variation in thermophysical properties and drift velocity correction is shown to increase uncertainty in the accommodation coefficient. Assuming an isothermal interface is not recommended since it causes inherent variability based on sampling statistics and introduces material/geometric dependencies.

To the authors' best knowledge the data presented here are the first known measurements of the mass accommodation coefficients for cryogenic hydrogen and methane. These values are critical to developing space infrastructure for the upcoming Lunar and Martian missions. The Schrage expression adapted for curved interfaces (Eqs. (10) and (15)) includes the effect of drift velocity, curvature, disjoining pressure and local variation in thermophysical properties. The agreement between $\hat{\alpha}$ with transition state theory suggests that the coefficient can be well-characterized and may even be fluid independent. Further evidence of agreement with other (non-cryogenic) fluids is needed.

CRediT authorship contribution statement

Kishan Bellur: Investigation, Methodology, Formal analysis, Writing – original draft. **Ezequiel F. Médici:** Investigation, Methodology. **James C. Hermanson:** Conceptualization, Writing – review & editing. **Chang Kyoung Choi:** Conceptualization, Supervision. **Jeffrey S. Allen:** Conceptualization, Supervision, Project Administration, Writing – review & editing.

Declaration of competing interest

The authors declare the following financial interests/personal relationships which may be considered as potential competing interests: Jeffrey S. Allen, Chang Kyoung Choi, James C. Hermanson reports financial support was provided by NASA.

Data availability

Data will be made available on request.

Acknowledgments

References

[1] K. Bellur, E.F. Médici, M. Kulshreshtha, V. Konduru, D. Tyrewala, A. Tamilarasan, J. McQuillen, J.B. Leão, D.S. Hussey, D.L. Jacobson, J. Scherschligt, J.C. Hermanson, C.K. Choi, J.S. Allen, A new experiment for investigating evaporation and condensation of cryogenic propellants, Cryogenics (ISSN: 00112275) 74 (2016) 131–137, http://dx.doi.org/10.1016/j.cryogenics.2015.10.016.

[2] Kishan Bellur, Ezequiel F. Médici, Chang Kyoung Choi, James C. Hermanson, Jeffrey S. Allen, Multiscale approach to model steady meniscus evaporation in a wetting fluid, Phys. Rev. Fluids 5 (2) (2020) 024001, http://dx.doi.org/10.1103/PhysRevFluids.5.024001.

[3] M.A. Saxton, D. Vella, J.P. Whiteley, J.M. Oliver, Kinetic effects regularize the mass-flux singularity at the contact line of a thin evaporating drop, J. Eng. Math. 106 (1) (2017) 47–73, http://dx.doi.org/10.1007/s10665-016-9892-4, (ISSN: 0022-0833, 1573-2703).

[4] H. Hertz, Ueber Die Verdunstung Der Flüssigkeiten, Insbesondere Des Quecksilbers, Im Luftleeren Raume, Ann. Phys. 253 (1882) 177–193, http://dx.doi.org/10.1002/andp.18822531002.

[5] R.W. Schrage, A Theoretical Study of Interphase Mass Transfer (Ph.D. thesis), Columbia University Press, 1953.

[6] Samantha J. Alberts, Praveen Srikanth, Steven H. Collicott, Stephen D. Heister, Numerical approach to measure accommodation coefficients for long-duration spaceflight cryogenic propellants, in: 52nd AIAA/SAE/ASEE Joint Propulsion Conference, American Institute of Aeronautics and Astronautics, Salt Lake City, UT, ISBN: 978-1-62410-406-0, 2016, http://dx.doi.org/10.2514/6.2016-4675.

[7] Samantha J. Alberts, Praveen Srikanth, Steven H. Collicott, Stephen D. Heister, Experiment design for measuring accommodation coefficients for modeling of long-duration spaceflight cryogenic propellants, in: 13th International Energy Conversion Engineering Conference, American Institute of Aeronautics and Astronautics, Orlando, FL, ISBN: 978-1-62410-376-6, 2015, http://dx.doi.org/10.2514/6.2015-4246.

[8] C.E. Kolb, R.A. Cox, J.P.D. Abbatt, M. Ammann, E.J. Davis, D.J. Donaldson, B.C. Garrett, C. George, P.T. Griffiths, D.R. Hanson, M. Kulmala, G. McFiggans, U. Pöschl, I. Riipinen, M.J. Rossi, Y. Rudich, P.E. Wagner, P.M. Winkler, D.R. Worsnop, C.D. O' Dowd, An overview of current issues in the uptake of atmospheric trace gases by aerosols and clouds, Atmos. Chem. Phys. (ISSN: 1680-7324) 10 (21) (2010) 10561–10605, http://dx.doi.org/10.5194/acp-10-10561-2010.

[9] Hans R. Pruppacher, James D. Klett, Pao K. Wang, Microphysics of clouds and precipitation, Aerosol Sci. Technol. 28 (4) (1998) 381–382, http://dx.doi.org/10.1080/02786829808965531, (ISSN: 0278-6826, 1521-7388).

[10] Michael Mozurkewich, Aerosol growth and the condensation coefficient for water: A review, Aerosol Sci. Technol. 5 (2) (1986) 223–236.

[11] B. Paul, Compilation of evaporation coefficients, ARS J. (ISSN: 1936-9972) 32 (9) (1962) 1321–1328, http://dx.doi.org/10.2514/8.6277.

[12] Dhruv Singh, Xiaohui Guo, Alina Alexeenko, Jayathi Y. Murthy, Timothy S. Fisher, Modeling of subcontinuum thermal transport across semiconductor-gas interfaces, J. Appl. Phys. (ISSN: 0021-8979) 106 (2) (2009) 024314, http://dx.doi.org/10.1063/1.3181059.

[13] V.P. Carey, G. Chen, C. Grigoropoulos, M. Kaviany, A. Majumdar, A review of heat transfer physics, Nanoscale Microscale Thermophys. Eng. (ISSN: 1556-7265) 12 (1) (2008) 1–60, http://dx.doi.org/10.1080/15567260801917520.

[14] D. Bayer, A new facility for the experimental investigation on nano heat transfer between gas molecules and ceramic surfaces, in: 32nd International Thermal Conductivity Conference, Purdue University, West Lafayette, Indiana, USA, 2014, p. 8, http://dx.doi.org/10.5703/1288284315549.

[15] D.R. Haynes, N.J. Tro, S.M. George, Condensation and evaporation of water on ice surfaces, J. Phys. Chem. 96 (21) (1992) 8502–8509, http://dx.doi.org/10.1021/j100200a055, (ISSN: 0022-3654, 1541-5740).

[16] R. Marek, J. Straub, Analysis of the evaporation coefficient and the condensation coefficient of water, Int. J. Heat Mass Transfer 44 (1) (2001) 39–53.

[17] E.J. Davis, A history and state-of-the-art of accommodation coefficients, Atmos. Res. (ISSN: 01698095) 82 (3–4) (2006) 561–578, http://dx.doi.org/10.1016/j.atmosres.2006.02.013.

[18] G.T. Barnes, The effects of monolayers on the evaporation of liquids, Adv. Colloid Interface Sci. (ISSN: 00018686) 25 (1986) 89–200, http://dx.doi.org/10.1016/0001-8686(86)80004-5.

[19] Yigit Akkus, Akif Turker Gurer, Kishan Bellur, Drifting mass accommodation coefficients: In situ measurements from a steady state molecular dynamics setup, Nanoscale Microscale Thermophys. Eng. (ISSN: 1556-7265) 25 (1) (2020) 25–45, http://dx.doi.org/10.1080/15567265.2020.1861139.

[20] Praveen Srikanth, Steven H. Collicott, Estimation of thin-film contribution in phase change calculations involving cryogenic propellants, J. Spacecr. Rockets (ISSN: 0022-4650) 56 (5) (2019) 1646–1650, http://dx.doi.org/10.2514/1.A34495.

[21] Mohammad Kassemi, Olga Kartuzova, Effect of interfacial turbulence and accommodation coefficient on CFD predictions of pressurization and pressure control in cryogenic storage tank, Cryogenics (ISSN: 00112275) 74 (2016) 138–153, http://dx.doi.org/10.1016/j.cryogenics.2015.10.018.

[22] C. Ludwig, M.E. Dreyer, Investigations on thermodynamic phenomena of the active-pressurization process of a cryogenic propellant tank, Cryogenics (ISSN: 00112275) 63 (2014) 1–16, http://dx.doi.org/10.1016/j.cryogenics.2014.05.005.

[23] Olga V. Kartuzova, Mohammad Kassemi, CFD modeling of the multipurpose hydrogen test bed (MHTB) self-pressurization and spray bar mixing experiments in normal gravity: effect of the accommodation coefficient on the tank pressure, in: 51st AIAA/SAE/ASEE Joint Propulsion Conference, American Institute of Aeronautics and Astronautics, Orlando, FL, ISBN: 978-1-62410-321-6, 2015, http://dx.doi.org/10.2514/6.2015-3769.

[24] Kishan Bellur, Vinaykumar Konduru, Manan Kulshrestha, Daanish Tyrewala, Ezequiel Medici, Jeffrey S. Allen, Chang Kyoung Choi, Daniel S. Hussey, David C. Jacobson, Juscelino B. Leão, John McQuillen, James Hermanson, Arun Tamilarasan, Contact angle measurement of liquid hydrogen (LH2) in stainless steel and aluminum cells, J. Heat Transfer (ISSN: 0022-1481) 138 (2) (2016) http://dx.doi.org/10.1115/1.4032232.

[25] Kishan Bellur, An Assessment of the Validity of the Kinetic Model for Liquid-Vapor Phase Change by Examining Cryogenic Propellants (Ph.D. thesis), Michigan Technological University, 2016.

[26] K. Bellur, E.F. Médici, J.C. Hermanson, C.K. Choi, J.S. Allen, Determining solid-fluid interface temperature distribution during phase change of cryogenic propellants using transient thermal modeling, Cryogenics (ISSN: 0011-2275) 91 (2018) 103–111, http://dx.doi.org/10.1016/j.cryogenics.2018.02.009.

[27] Kishan Bellur, Ezequiel F. Médici, Daniel S. Hussey, David L. Jacobson, Jacob LaManna, Juscelino B. Leão, Julia Scherschligt, James C. Hermanson, Chang Kyoung Choi, Jeffrey S. Allen, Results from neutron imaging phase change experiments with LH2 and LCH4, Cryogenics (ISSN: 0011-2275) 125 (2022) 103517, http://dx.doi.org/10.1016/j.cryogenics.2022.103517.

[28] Kishan Bellur, Ezequiel F. Medici, Daniel S. Hussey, David L. Jacobson, Jacob LaManna, Juscelino B. Leao, Julia Scherschligt, James C Hermanson, Chang Kyoung Choi, Jeffrey S. Allen, Data from cryo-neutron phase change experiments with LH2 and LCH4, Data Brief (ISSN: 2352-3409) 43 (2022) 108474, http://dx.doi.org/10.1016/j.dib.2022.108474.

[29] V.P. Carey, Liquid Vapor Phase Change Phenomena: An Introduction to the Thermophysics of Vaporization and Condensation Processes in Heat Transfer Equipment, CRC Press, 2007.

[30] I.W. Eames, N.J. Marr, H. Sabir, The evaporation coefficient of water: A review, Int. J. Heat Mass Transfer (ISSN: 00179310) 40 (12) (1997) 2963–2973, http://dx.doi.org/10.1016/S0017-9310(96)00339-0.

[31] M. Knudsen, Maximum rate of vaporization of mercury, Ann. Phys. 47 (1915) 697–705.

[32] Van P. Carey, Statistical Thermodynamics and Microscale Thermophysics, Cambridge University Press, 1999.

[33] P. Davidovits, D.R. Worsnop, J.T. Jayne, C.E. Kolb, P. Winkler, A. Vrtala, P.E. Wagner, M. Kulmala, K.E.J. Lehtinen, T. Vesala, M. Mozurkewich, Mass accommodation coefficient of water vapor on liquid water: Mass accommodation, Geophys. Res. Lett. (ISSN: 00948276) 31 (22) (2004) http://dx.doi.org/10.1029/2004GL020835.

[34] P.C. Wayner, The effect of interfacial mass transport on flow in thin liquid films, Colloids Surf. 52 (1991) 71–84.

[35] S. DasGupta, I.Y. Kim, P.C. Wayner, Use of the kelvin-clapeyron equation to model an evaporating curved microfilm, J. Heat Transfer (ISSN: 0022-1481) 116 (4) (1994) 1007–1015, http://dx.doi.org/10.1115/1.2911436.

[36] P.C. Wayner, Y.K. Kao, L.V. LaCroix, The interline heat-transfer coefficient of an evaporating wetting film, Int. J. Heat Mass Transfer 19 (1976) 487–492.

[37] A.H. Persad, C.A. Ward, Expressions for the evaporation and condensation coefficients in the Hertz-Knudsen relation, Chem. Rev. 116 (14) (2016) 7727–7767.

[38] Paul Davidovits, Charles E. Kolb, Leah R. Williams, John T. Jayne, Douglas R. Worsnop, Update 1 of: Mass accommodation and chemical reactions at gas-liquid interfaces, Chem. Rev. 111 (4) (2011) cr100360b, http://dx.doi.org/10.1021/cr100360b, (ISSN: 0009-2665, 1520-6890).

[39] H.K. Cammenga, H. Klinge, B.-E. Rudolph, Untersuchungen über die Verdampfungs-Geschwindigkeit von Flüssigkeiten, Fortschrittsberichte Über Kolloide Und Polymere (ISSN: 0071-8017) 55 (1) (1971) 118–123, http://dx.doi.org/10.1007/BF02826279.

[40] Masataka Okuyama, Joseph T. Zung, Evaporation—condensation coefficient for small droplets, J. Chem. Phys. 46 (5) (1967) 1580–1585, http://dx.doi.org/10.1063/1.1840906, (ISSN: 0021-9606, 1089-7690).

[41] Jonathan Barrett, Charles Clement, Kinetic evaporation and condensation rates and their coefficients, J. Colloid Interface Sci. (ISSN: 00219797) 150 (2) (1992) 352–364, http://dx.doi.org/10.1016/0021-9797(92)90205-Z.

[42] Paul L. Barclay, Jennifer R. Lukes, Curvature dependence of the mass accommodation coefficient, Langmuir : ACS J. Surf. Colloids 35 (18) (2019) 6196–6202, http://dx.doi.org/10.1021/acs.langmuir.9b00537, (ISSN: 0743-7463, 1520-5827).

[43] G. Burrows, Evaporation at low pressures, J. Appl. Chem. 7 (7) (1957) 375–384, http://dx.doi.org/10.1002/jctb.5010070706, (ISSN: 00218871, 1934998X).

[44] G. Burrows, Molecular Distillation, Oxford University Press, 1960.

[45] G. Burrows, Evaporation in an evacuated container, Vacuum (ISSN: 0042-207X) 15 (8) (1965) 389–399, http://dx.doi.org/10.1016/0042-207X(65)90482-3.

[46] G. Burrows, Notes on some features of high-vacuum distillation, Vacuum (ISSN: 0042-207X) 23 (10) (1973) 353–358, http://dx.doi.org/10.1016/0042-207X(73)90490-9.

[47] J. Kapłon, Z. Kawala, A. Skoczylas, Evaporation rate of a liquid from the surface of a rotating disc in high vacuum, Chem. Eng. Sci. (ISSN: 00092509) 41 (3) (1986) 519–522, http://dx.doi.org/10.1016/0009-2509(86)87033-6.

[48] C.E. Bryson, V. Cazcarra, M. Chouarain, L.L. Levenson, High-precision measurements of condensation coefficients. results for carbon dioxide and water molecules, J. Vac. Sci. Technol. (ISSN: 0022-5355) 9 (1) (1972) 557–560, http://dx.doi.org/10.1116/1.1316684.

[49] C.E. Bryson, V. Cazcarra, L.L. Levenson, Condensation coefficient measurements of H2O, N2O, and CO2, J. Vac. Sci. Technol. (ISSN: 0022-5355) 11 (1) (1974) 411–416, http://dx.doi.org/10.1116/1.1318639.

[50] Robert Hołyst, Marek Litniewski, Daniel Jakubczyk, A molecular dynamics test of the Hertz–Knudsen equation for evaporating liquids, Soft Matter (ISSN: 1744-6848) 11 (36) (2015) 7201–7206, http://dx.doi.org/10.1039/C5SM01508A.

[51] Jer Ru Maa, The role of interfaces in heat transfer processes, Adv. Colloid Interface Sci. (ISSN: 0001-8686) 18 (3) (1983) 227–280, http://dx.doi.org/10.1016/0001-8686(83)87003-1.

[52] Sandra L. Lednovich, John B. Fenn, Absolute evaporation rates for some polar and nonpolar liquids, AIChE J. 23 (4) (1977) 454–459, http://dx.doi.org/10.1002/aic.690230408, (ISSN: 0001-1541, 1547-5905).

[53] T. Alty, Joseph John Thomson, The reflection of vapour molecules at a liquid surface, Proc. R. Soc. Lond. Ser. A Contain. Pap. A Math. Phys. Charact. 131 (818) (1931) 554–564, http://dx.doi.org/10.1098/rspa.1931.0072.

[54] T. Alty, F.H. Nicoll, The interchange of molecules between a liquid and its vapor, Can. J. Res. (ISSN: 1923-4287) 4 (6) (1931) 547–558, http://dx.doi.org/10.1139/cjr31-041.

[55] T. Alty, C.A. Mackay, Ralph Howard Fowler, The accommodation coefficient and the evaporation coefficient of water, Proc. R. Soc. Lond. Ser. A Math. Phys. Sci. 149 (866) (1935) 104–116, http://dx.doi.org/10.1098/rspa.1935.0050.

[56] A.M. Sinnarwalla, D.J. Alofs, J.C. Carstens, Measurement of growth rate to determine condensation coefficients for water drops grown on natural cloud nuclei, J. Atmos. Sci. (ISSN: 0022-4928) 32 (3) (1975) 592–599, http://dx.doi.org/10.1175/1520-0469(1975)032<0592:MOGRTD>2.0.CO;2.

[57] V.K. Badam, V. Kumar, F. Durst, K. Danov, Experimental and theoretical investigations on interfacial temperature jumps during evaporation, Exp. Therm Fluid Sci. 32 (1) (2007) 276–292, http://dx.doi.org/10.1016/j.expthermflusci.2007.04.006.

[58] P.M. Winkler, A. Vrtala, R. Rudolf, P.E. Wagner, I. Riipinen, T. Vesala, K.E.J. Lehtinen, Y. Viisanen, M. Kulmala, Condensation of water vapor: Experimental determination of mass and thermal accommodation coefficients, J. Geophys. Res.-Atmos. 111 (D19) (2006).

[59] M. Potash, P.C. Wayner Jr., Evaporation from a two-dimensional extended meniscus, Int. J. Heat Mass Transfer (ISSN: 00179310) 15 (10) (1972, 1972-10) 1851–1863, http://dx.doi.org/10.1016/0017-9310(72)90058-0.

[60] J.A. Schonberg, S. DasGupta, P.C. Wayner, An augmented Young-Laplace model of an evaporating meniscus in a microchannel with high heat flux, Aerospace Heat Exchanger Technology, Exp. Therm Fluid Sci. (ISSN: 0894-1777) 10 (2) (1995) 163–170, http://dx.doi.org/10.1016/0894-1777(94)00085-m.

[61] Sang-Kwon Wee, Kenneth D. Kihm, David M. Pratt, Jeffrey S. Allen, Microscale heat and mass transport of evaporating thin film of binary mixture, J. Thermophys. Heat Transfer 20 (2) (2006) 320–326, http://dx.doi.org/10.2514/1.15784, (ISSN: 0887-8722, 1533-6808).

[62] David M. Pratt, Kevin P. Hallinan, Thermocapillary effects on the wetting characteristics of a heated curved meniscus, J. Thermophys. Heat Transfer (ISSN: 0887-8722) 11 (4) (1997) 519–525, http://dx.doi.org/10.2514/2.6293.

[63] Peter C. Wayner Jr., Interfacial forces and phase change in thin liquid films, in: Tien, Mujumdar, Gerner (Eds.), Microscale Energy Transport, Tayler & Francis, 1998, pp. 187–224.

[64] P.C. Wayner, Intermolecular forces in phase-change heat transfer: 1998 Kern award review, AIChE J. 45 (10) (1999) 2055–2068.

[65] Kishan Bellur, Vinaykumar Konduru, Ezequiel F. Medici, Daniel S. Hussey, David L. Jacobson, Jacob M. LaManna, Jeffrey S. Allen, Chang Kyoung Choi, Visualization of the evaporation and condensation phenomena in cryogenic propellants, J. Flow Vis. Image Process. 23 (1–2) (2016) http://dx.doi.org/10.1615/JFlowVisImageProc.2017020115, (ISSN: 1065-3090, 1940-4336).

[66] Kishan Bellur, A New Technique to Determine Accommodation Coefficients of Cryogenic Propellants (Ph.D. thesis), Michigan Technological University, 2018.

[67] Shengfeng Cheng, Jeremy B. Lechman, Steven J. Plimpton, Gary S. Grest, Evaporation of Lennard-Jones fluids, J. Chem. Phys. (ISSN: 0021-9606) 134 (22) (2011) 224704, http://dx.doi.org/10.1063/1.3595260.

[68] Zhi Liang, Thierry Biben, Pawel Keblinski, Molecular simulation of steady-state evaporation and condensation: Validity of the Schrage relationships, Int. J. Heat Mass Transfer (ISSN: 0017-9310) 114 (2017) 105–114, http://dx.doi.org/10.1016/j.ijheatmasstransfer.2017.06.025.

[69] A. Lotfi, J. Vrabec, J. Fischer, Evaporation from a free liquid surface, Int. J. Heat Mass Transfer 73 (2014) 303–317.

[70] G. Nagayama, T. Tsuruta, A general expression for the condensation coefficient based on the transition state theory and molecular dynamics simulation, J. Chem. Phys. 118 (3) (2003) 1392–1399.

[71] G. Nagayama, M. Takematsu, H. Mizuguchi, T. Tsuruta, Molecular dynamics study on Condensation/Evaporation coefficients of chain molecules at Liquid–Vapor interface, J. Chem. Phys. 143 (2015) 014706.

[72] Frank D. Maslan, Theodore M. Littman, Compressibility chart for hydrogen and inert gases, Ind. Eng. Chem. 45 (7) (1953) 1566–1568, http://dx.doi.org/10.1021/ie50523a054, (ISSN: 0019-7866, 1541-5724).

[73] S.A. Sherif, N. Zeytinoglu, T.N. Veziroğlu, Liquid hydrogen: Potential, problems, and a proposed research program, Int. J. Hydrogen Energy (ISSN: 0360-3199) 22 (7) (1997) 683–688, http://dx.doi.org/10.1016/S0360-3199(96)00201-7.

[74] A.M. Juarez, D. Cubric, G.C. King, A compact catalytic converter for the production of para-hydrogen, Meas. Sci. Technol. (ISSN: 09570233) 13 (5) (2002) N52–N55, http://dx.doi.org/10.1088/0957-0233/13/5/402.